Chinese Journal of Catalysis 36 (2015) 1392–1402

available at www.sciencedirect.com

ScienceDirect

journal homepage: www.elsevier.com/locate/chnjc

Article

Methanol to hydrocarbons reaction over HZSM-22 and SAPO-11: Effect of catalyst acid strength on reaction and deactivation mechanism

Jinbang Wang [a,b,d], Jinzhe Li [b], Shutao Xu [b], Yuchun Zhi [b], Yingxu Wei [b,#], Yanli He [b], Jingrun Chen [b,d], Mozhi Zhang [b,d], Quanyi Wang [b], Wenna Zhang [b,d], Xinqiang Wu [b,d], Xinwen Guo [a,*], Zhongmin Liu [b,c,$]

[a] *State Key Laboratory of Fine Chemicals, PSU-DUT Joint Center for Energy Research, School of Chemical Engineering, Dalian University of Technology, Dalian 116024, Liaoning, China*

[b] *National Engineering Laboratory for Methanol to Olefins, State Energy Low Carbon Catalysis and Engineering R&D Center, Dalian National Laboratory for Clean Energy, iChEM (Collaborative Innovation Center of Chemistry for Energy Materials), Dalian Institute of Chemical Physics, Chinese Academy of Sciences, Dalian 116023, Liaoning, China*

[c] *State Key Laboratory of Catalysis, Dalian Institute of Chemical Physics, Chinese Academy of Sciences, Dalian 116023, Liaoning, China*

[d] *University of Chinese Academy of Sciences, Beijing 100049, China*

ARTICLE INFO

Article history:
Received 26 May 2015
Accepted 9 July 2015
Published 20 August 2015

Keywords:
HZSM-22
SAPO-11
Methanol-to-hydrocarbon
Acid strength
Mechanism

ABSTRACT

The conversion of methanol to hydrocarbons has been investigated over HZSM-22 and SAPO-11. Both of these catalysts possess one-dimensional 10-ring channels, but have different acidic strengths. Comparison studies and $^{12}C/^{13}C$ isotopic switching experiments were conducted to evaluate the influence of the acidic strength of the catalyst on the conversion of methanol, as well as its deactivation mechanism. Although the conversion of methanol proceeded via an alkene methylation-cracking pathway over both catalysts, the acidity of the catalysts had a significant impact on the conversion and product distribution of these reactions. The stability of the catalysts varied with temperature. The catalysts were deactivated at high temperature by the deposition of graphitic coke on their outer surface. Deactivation also occurred at low temperatures a result that the pores of the catalyst were blocked by polyaromatic compounds. The co-reaction of ^{13}C-methanol and ^{12}C-1-butene confirmed the importance of the acidity of the catalyst on the distribution of the hydrocarbon products.

© 2015, Dalian Institute of Chemical Physics, Chinese Academy of Sciences.
Published by Elsevier B.V. All rights reserved.

1. Introduction

Light alkenes and liquid hydrocarbon fuels are important petrochemical commodities, and the majority of the compounds belonging to these groups are produced through petrochemical reactions. Dwindling oil supplies and the rapidly increasing demand for fuels and light alkenes have stimulated significant research efforts towards the development of new processes for the production of these petrochemical products from alternative and abundant resources, such as biomass, coal and natural gas [1,2]. Among these non-petrochemical routes, the methanol-to-hydrocarbon (MTH) route has become a suc-

* Corresponding author. Tel: +86-411-84986133; Fax: +86-411-84986134; E-mail: guoxw@dlut.edu.cn
# Corresponding author. Tel: +86-411-84379118; E-mail: weiyx@dicp.ac.cn
$ Corresponding author. Tel: +86-411-84379335; E-mail: liuzm@dicp.ac.cn
This work was supported by the National Natural Science Foundation of China (201473182, 21273005, 21273230, 21103180).
DOI: 10.1016/S1872-2067(15)60953-6 | http://www.sciencedirect.com/science/journal/18722067 | Chin. J. Catal., Vol. 36, No. 8, August 2015

cessful commercial process [2–4]. Furthermore, a wide range of different zeolites have been investigated as catalysts for the MTH reaction during the past decades [2,3,5], including ZSM-5 and SAPO-34, which are believed to be the most effective catalysts for this process. These catalysts have also been applied to a variety of commercial processes, including methanol-to-olefin (MTO) [4,6], methanol-to-propene (MTP) [7] and methanol-to-gasoline (MTG) [8–10] processes.

Considerable research efforts have also been devoted to developing a deeper understanding of the mechanism of the MTH reaction. The results of previous investigations have shown that the detailed mechanism of the MTH reaction is very complicated and strongly dependent on the topology of the zeolite catalyst. For example, SAPO-34, which consists of large supercages and small 8-ring windows, is currently regarded as the best catalyst for MTO reactions [4,11]. It is noteworthy that the high level of selectivity exhibited by this catalyst for ethene and propene has been attributed to the hydrocarbon pool mechanism [12–14]. Furthermore, polymethylbenzene and polymethylcyclopentadiene, as well as their protonated analogues, have been reported to be important reactive intermediates for the production of alkenes [15–22]. The formation of these bulky intermediates was not only observed over SAPO-34 but was also detected in several other zeolites with wide or intersectional channels, such as Hβ [23], ZSM-5 [20], SSZ-13 [19] and DNL-6 [24,25]. In a separate study, Svelle et al. [26–28] conducted a series of $^{12}C/^{13}C$-methanol labeling experiments over the medium pore acidic zeolite ZSM-5 to show that the generation of ethene occurred via an separated route, independent of the one responsible for the formation of C_3^+ alkenes. The authors went on to propose a dual-cycle mechanism for this transformation, which consists of an aromatic-based cycle with xylene/triMB as reactive intermediates for the production of ethene and a C_3^+ alkene-based cycle for the formation of propene and higher alkenes. Based on this mechanistic insight, there have been considerable researches about whether the conversion of methanol could run in an independent manner while suppressing the formation of ethene via an alkene cycle by carefully controlling the topology of the catalyst [26]. This assumption was recently validated over the one-dimensional 10-ring zeolite, HZSM-22, which produces hydrocarbons rich in C_5^+ branched alkenes and low in aromatics and ethene [29–32].

In addition to their topological characteristics, the acidic properties of zeolite catalysts can also have a significant impact on their performances for the conversion of methanol. This issue was first reported by Yuen et al. [33] over CHA and AFI catalysts. The results of this study revealed that the acidity of borosilicate sieves was too low to allow for the conversion of methanol to hydrocarbons, and that SAPO-34 displayed lower hydrogen transfer reactivity than SSZ-13. Most recently, Bleken et al. [34] reported the systematic comparison of SAPO-34 and SSZ-13 in the MTO reaction. The results showed that the more acidic SSZ-13 catalyst exhibited higher activity, which leads to a higher methanol conversion than that of the less acidic SAPO-34 catalyst under the same operating conditions. Westgård Erichsen et al. [35] also conducted a comparative study to determine the effects of the acidic strength of the catalyst on MTO reactions over AFI and SAPO zeolite catalysts. The results showed that the use of a catalyst with a low acidic strength promoted the conversion of methanol via an alkene-mediated mechanism. Taken together, these results show that it is of critical importance to understand the detailed role played by the acidic properties of these catalysts in the formation of alkenes. Furthermore, the performance characteristics of these catalysts could be optimized by tuning their acidic properties, representing an alternative approach to the optimization of these processes, which should therefore be explored in greater detail.

In this study, we have used two one-dimensional 10-ring zeolites, HZSM-22 (TON, 0.46 × 0.57 nm) and SAPO-11 (AEL, 0.4 × 0.65 nm), to elucidate the role of their acidic strength on the MTH reaction and their deactivation mechanism.

2. Experimental

2.1. Catalyst preparation

The K-ZSM-22 and SAPO-11 catalysts were supplied by Group DNL0802 of the Dalian Institute of Chemical Physics, Dalian, China. After being calcined at 600 °C for 10 h to remove the organic template, K-ZSM-22 was converted to NH_4-ZSM-22 by three ion-exchange processes in a NH_4NO_3 solution (1 mol/L) at 80 °C for 6 h. The resulting catalyst was then washed with deionized water, dried over night at 120 °C and calcined at 550 °C for 4 h to give protonated H-ZSM-22. The SAPO-11 sample was calcined at 550 °C for 4 h to give H-SAPO-11.

2.2. Catalyst characterization

The structural properties of two catalysts were characterized using a PANalytical X'Pert PRO X-ray diffraction (XRD) system with Cu K_α radiation (λ = 0.154059 nm) at 40 kV and 40 mA. The chemical compositions of the catalysts were determined using a Philips Magix-601 X-ray fluorescence (XRF) spectrometer. The morphological characteristics of the catalysts were measured by field emission scanning electron microscopy (FE-SEM) on a Hitachi SU8020 system.

The N_2 physisorption isotherms of the samples were measured at –196 °C on a Micromeritics ASAP 2020 system. Fresh samples of the catalysts were degassed under vacuum at 90 °C for 1 h and then at 350 °C for 3 h before being analyzed. The surface areas of the samples were calculated using the Brunauer-Emmett-Teller (BET) equation, and their micropore volumes were evaluated using the *t*-plot method.

The spent catalysts were collected and analyzed by thermogravimetric analysis (TGA) on a Q500 SDT thermogravimetric analyzer. In a typical measurement, a small sample (10–14 mg) of spent catalyst was heated in an Al_2O_3 crucible from ambient temperature to 900 °C at a heating rate of 10 °C/min under a stream of air at a constant flow rate of 100 ml/min.

The acidity of the catalysts was determined by the temperature programmed desorption of ammonia (NH_3-TPD) on a Micromeritics AutoChem 2920 system. The samples were

loaded in a U-shaped micro-reactor and pretreated at 650 °C for 30 min under an atmosphere of He. After cooling to 100 °C, the samples were saturated with NH_3, followed by purging with helium to remove the physisorbed NH_3. The desorption experiments were conducted under a stream of He (40 ml/min) by increasing the temperature from 100 to 600 °C at a ramp rate of 10 °C/min. The TPD signals were monitored simultaneously using a thermal conductivity detector (TCD).

^{1}H MAS NMR experiments were carried out on a Bruker Avance III 600 spectrometer equipped with a 14.1 T wide-bore magnet and a 4 mm magic angle spinning (MAS) probe (Bruker). The details of this procedure have been reported elsewhere [36]. Briefly, the samples were dehydrated at 400 °C for 20 h at a pressure of less than 10^{-3} Pa prior to the adsorption of perfluorotributylamine. The selective adsorption of perfluorotributylamine was performed by exposing the dehydrated samples to a saturated vapor at room temperature for 30 min. The samples were then degassed to remove any physical adsorbates from their surfaces. Dehydrated samples both with and without the perfluorotributylamine adsorption were then measured by ^{1}H MAS NMR spectroscopy to determine their acidic sites distributions.

2.3. Catalytic tests

200 mg samples of the catalysts were pressed, sieved through a 40–60 mesh and then loaded into a fixed-bed stainless tubular reactor with an inner diameter of 6 mm. Prior to the catalytic measurements, the catalysts were activated at 500 °C for 1 h, and the temperature was then adjusted to the appropriate reaction temperature. All of the reactions were conducted under atmospheric pressure. Saturated methanol vapor was fed into the reactor by passing the carrier gas (He) through a saturator, which was maintained at 40 °C. The effluent products inside the transfer line were kept at 120 °C and analyzed by online gas chromatography (GC) on a Bruker GC450 system equipped with a PoraPLOT Q-HT capillary column and a FID detector. The conversion and selectivity of the catalysts were calculated on CH_2 basis and methanol and dimethyl ether were both considered to be reactants based on their rapid interconversion.

For the ^{12}C/^{13}C-methanol isotopic switching experiments, ^{12}C-methanol was fed through a saturator maintained at 14 °C for 15 min under a steady stream of He (12.4 ml/min). The reactant was switched to ^{13}C-methanol for 1 min and the reaction was then stopped. The catalyst particles were subsequently transferred to a vessel containing liquid nitrogen for rapid cooling. The discharged catalysts were dissolved in HF solution (20%) and the organic materials trapped in the catalyst were extracted with dichloromethane and subsequently analyzed by GC-MS on an Agilent 7890A/5975C GC/MSD system [37].

In the co-reaction of ^{13}C-methanol with ^{12}C-alkenes, methanol, which was fed through a saturator at 20 °C using a carrier gas (17.6 ml/min) with a weight hourly space velocity (WHSV) of 3 h^{-1}, was mixed with a stream of alkenes and introduced to a reactor. The ratios of methanol to the different alkenes were confirmed by GC analysis. The effluent products were analyzed using an online GC-MS system.

2.4. In situ FTIR

The Brönsted acidities and characteristics of the surface species during the MTH conversion over HZSM-22 were monitored using *in situ* FTIR spectroscopy on a Bruker Vextex70 infrared spectrometer. The catalyst was activated at 500 °C for 1 h prior to the reaction, and the temperature was subsequently adjusted to the required reaction temperature of 400 °C. After recording the spectrum of the activated catalyst, methanol was fed into the cell by passing the carrier gas (He, 20 ml/min) through a saturator containing methanol at 5 °C. The *in situ* FTIR spectra were recorded simultaneously with a resolution of 4 cm^{-1}.

3. Results and discussion

3.1. Characterization of the catalysts

The powder XRD patterns of the two samples (Fig. 1) matched well with the simulated patterns of the TON and AEL frameworks, which confirms that these catalysts possessed good crystallinity and phase purity characteristic. The Si/Al ratio of the HZSM-22 catalyst was determined to be 33 by XRF and the $n_{Si}/(n_{Si} + n_{Al} + n_P)$ value of the calcined SAPO-11 material was determined to be 0.13. Representative SEM micrographs of the catalysts (Fig. 2) revealed that the HZSM-22 catalyst existed as rod-like crystals with diameter and length measurement of 40 and 300 nm, respectively. In contrast, the SAPO-11 catalyst existed as flake-like crystals with dimensions of less than 2 μm. The N_2 adsorption-desorption isotherms of the two catalysts are shown in Fig. 3. Both catalysts gave a type I isotherm, which is typical of microporous materials. The specific BET surface areas, microporous surface areas and microporous volumes of the two catalysts are summarized in Table 1. These results show that HZSM-22 and SAPO-11 have comparable surface areas and pore volumes.

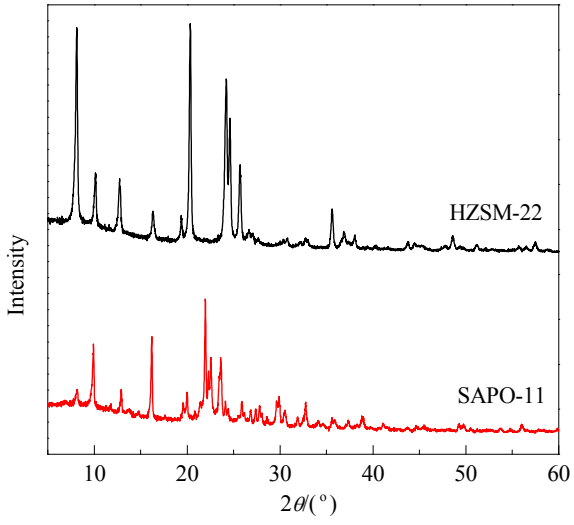

Fig. 1. XRD patterns of HZSM-22 and SAPO-11.

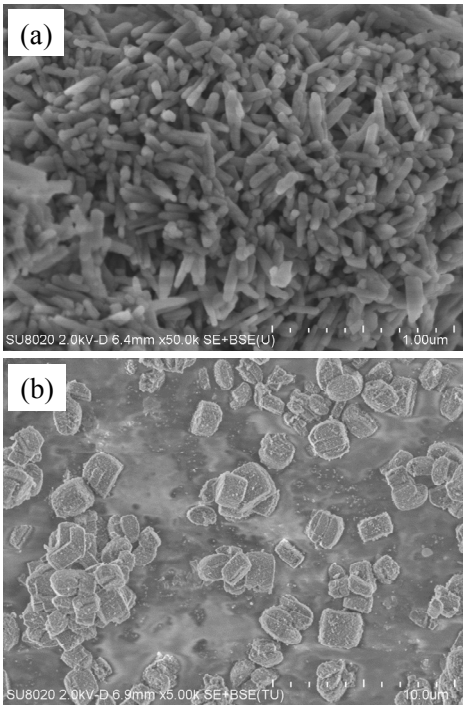

Fig. 2. SEM images of HZSM-22 (a) and SAPO-11 (b)

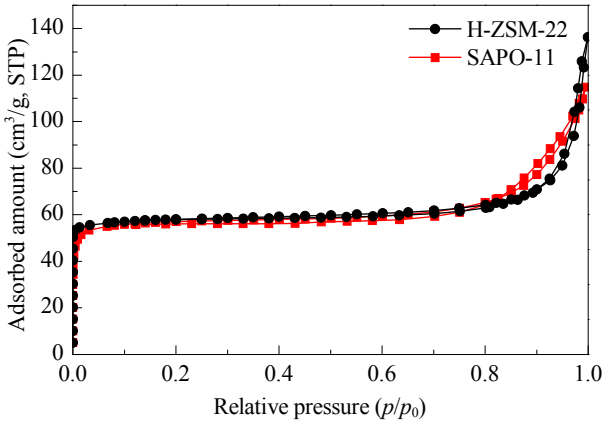

Fig. 3. N_2 adsorption-desorption isotherms of HZSM-22 and SAPO-11 recorded at –196 °C.

Table 1
Textual properties and Brönsted acidities of HZSM-22 and SAPO-11.

Sample	S_{BET}/ (m^2/g)	S_{micro}/ (m^2/g)	V_{micro}/ (cm^3/g)	Brönsted acid density (mmol/g)
HZSM-22	193	172	0.08	0.33
SAPO-11	191	165	0.08	0.23

The acidic properties of HZSM-22 and SAPO-11 were characterized by NH_3-TPD (Fig. 4). Both of these catalysts gave two desorption peaks corresponding to two distinct acidic strengths. For SAPO-11, the NH_3 desorption peaks centered at 160 and 280 °C were attributed to weak and moderate acidic sites, respectively. For HZSM-22, the desorption peaks at 200 and 410 °C were attributed to weak and relatively strong acidic sites, respectively. These results therefore revealed that the HZSM-22 catalyst was more acidic than the SAPO-11 catalyst.

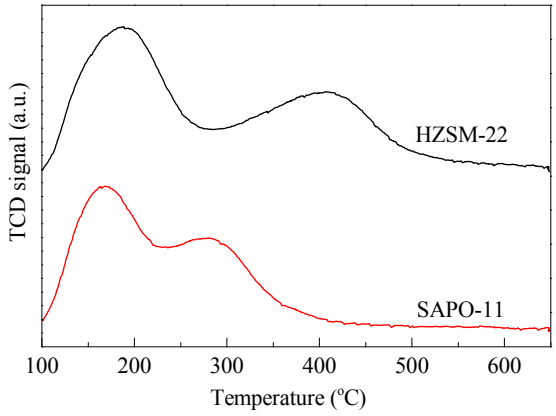

Fig. 4. NH_3-TPD profiles of HZSM-22 and SAPO-11.

According to the desorption areas measured under high temperature conditions, the acid density of the HZSM-22 catalyst was slightly higher than that of the SAPO-11 catalyst. Although a large number of Si atoms were incorporated into the SAPO-11 framework, the contribution of these atoms to the generation of Brönsted acidic sites was limited because of the formation of Si islands in the SAPO-11 catalyst [38,39].

The Brönsted acidities of HZSM-22 and SAPO-11 were also characterized by ^{1}H MAS NMR spectroscopy, and the resulting spectra are shown in Fig. 5. For HZSM-22, the signals at 3.9 and 6.1 ppm were attributed to the bridging hydroxyl groups (Si(OH)Al) and the disturbed bridging hydroxyl groups (Si(OH)Al), respectively, with the latter being influenced by an additional interaction with the oxygen atoms in the framework. Additional peaks were observed at 1.7 and 2.5 ppm, which were attributed to SiOH and AlOH, respectively [40–42]. For

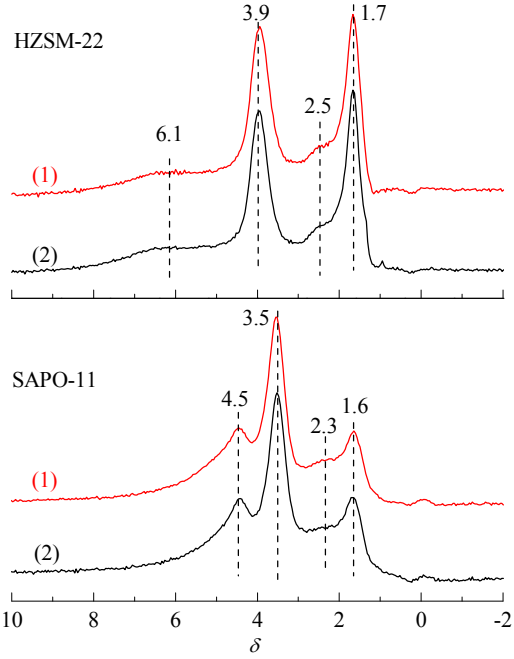

Fig. 5. ^{1}H MAS NMR of HZSM-22 and SAPO-11 before (1) and after (2) the adsorption of perfluorotributylamine.

SAPO-11, the signals at 3.5 and 4.5 ppm were attributed to the bridging hydroxyl groups (Si(OH)Al), whereas the signals at 1.6 and 2.3 ppm were assigned to SiOH and AlOH, respectively [38,42–44]. The signals of the bridging hydroxyl groups were indicative of the characteristic Brönsted acidic sites of the strongly acidic aluminosilicate zeolite (HZSM-22), as well as those of silicoaluminophosphate molecular sieves with medium strong acidity (SAPO-11). The results of the quantitative analysis given in Table 1 show that the concentration of Brönsted acidic sites in HZSM-22 (0.33 mmol/g) was a little higher than that of SAPO-11 (0.23 mmol/g). Moreover, perfluorotributylamine is a useful basic probe for distinguishing between the internal and external acidic sites in zeolites with the aid of ^{1}H MAS NMR [45]. Given that the diameter of perfluorotributylamine is 0.94 nm, and therefore much larger than the pore sizes of HZSM-22 and SAPO-11, this probe molecule could only be adsorbed by the acidic sites located on the external surfaces of these catalysts. The differences in the ^{1}H MAS NMR spectra of these catalysts both before and after the adsorption of perfluorotributylamine could be used to estimate the amount of acidic sites located on the external surfaces of the catalysts. The variations in the intensities of these spectra were very small, as shown in Fig. 5, which indicates that the majority of the acidic sites on both HZSM-22 and SAPO-11 were located on the internal surface, allowing for the meaningful comparison of the reactions carried out over these two catalysts.

3.2. Catalytic performances of HZSM-22 and SAPO-11 for the conversion of methanol

3.2.1. Methanol conversion and product distribution data

Figure 6 shows the methanol conversion profile with respect to time on stream over HZSM-22 and SAPO-11 at temperatures in the range of 350 to 550 °C. At the beginning of the reaction, methanol was completely converted to hydrocarbons over HZSM-22 at all of the reaction temperatures investigated. The time required for the complete conversion of methanol could be increased by increasing the temperature from 350 to 500 °C. However, further increasing the temperature up to 550 °C resulted in a reduction in the duration with 100% methanol conversion.

Compared with HZSM-22, SAPO-11 showed inferior reactivity for the conversion of methanol. Increasing the temperature from 350 to 500 °C led to an increase in the initial methanol conversion over SAPO-11 from 23 to 98%. It is noteworthy that the deactivation of the SAPO-11 catalyst was much slower at lower temperatures, even though the activity of this catalyst was also lower at lower temperatures. A sharp decrease was observed in the methanol conversion with time on stream above 400 °C, which indicates the rapid deactivation of the catalyst.

It was assumed that the significant differences observed in the initial conversion profiles of methanol over HZSM-22 and SAPO-11 could be correlated with their acidic properties. Furthermore, the experimental observations described above indicate that high acidic strength leads to high reactivity, which is in agreement with the results observed over SSZ-13 and SAPO-34 [34]. From the perspective of catalytic stability, HZSM-22 displayed a higher optimum temperature (500 °C) than that of SAPO-11 (400 °C).

Figure 7 shows the product distributions obtained over HZSM-22 and SAPO-11 at different reaction temperatures. Although both of these catalysts possess analogous topological structures, there were significant differences in the product distributions formed over the two catalysts. At 350–500 °C, C_5 and higher hydrocarbons were formed as the major products over SAPO-11. For HZSM-22, ethene and propene were generated as the major products, especially at relatively high reaction temperature of 450–550 °C. Ignoring the impact of the topology of the zeolite, the differences in the product distributions over the two catalysts could stem from the differences in the acidities of the catalysts. The stronger acidity of HZSM-22 compared with SAPO-11 would favors the generation of light alkenes and other hydrocarbon products, especially at higher temperature, whereas the lower acidity of SAPO-11 would favor the formation of higher hydrocarbons, such as C_{5+} hydro-

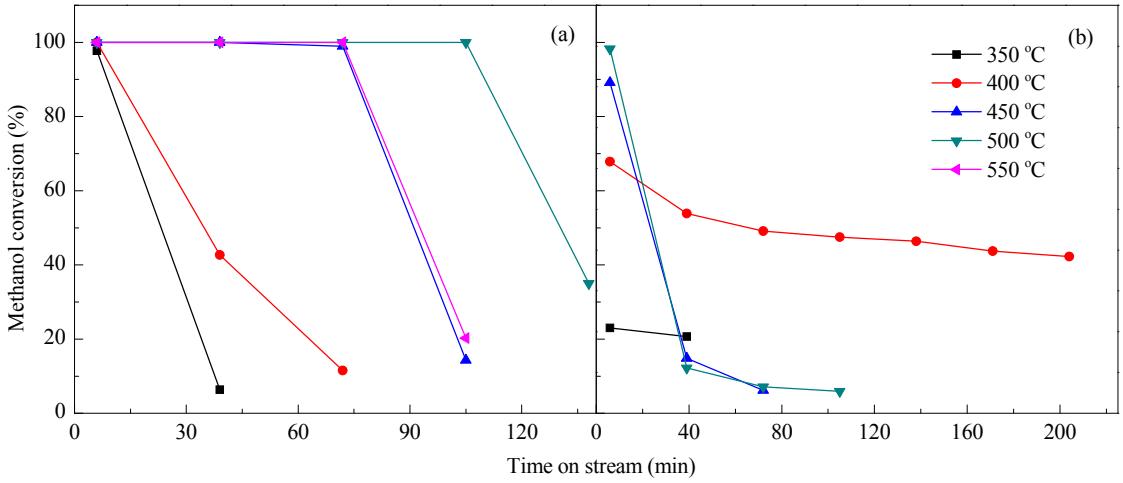

Fig. 6. Methanol conversion over HZSM-22 (a) and SAPO-11 (b) as a function of time on stream at various reaction temperatures with a methanol WHSV of 3.0 h^{-1} and a He/methanol ratio of 1.9.

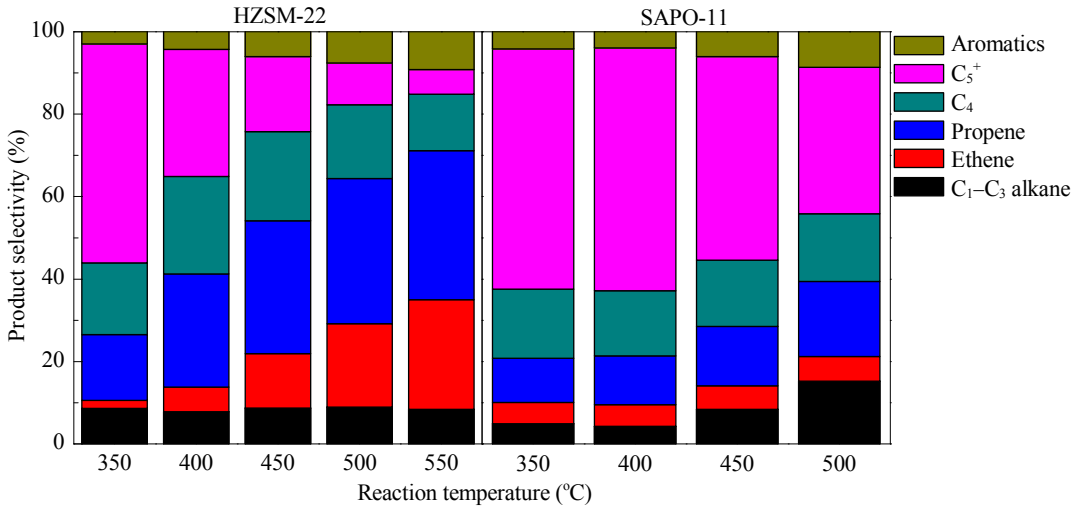

Fig. 7. Product selectivity of the methanol conversion process over HZSM-22 and SAPO-11 at various reaction temperatures with a methanol WHSV of 3.0 h^{-1} and a He/methanol ratio of 1.9.

carbons. As well as the acidities of the catalysts, the temperature of the reaction also had a significant impact on the product distribution. Over HZSM-22, C_5^+ hydrocarbons were formed as the main products below 400 °C, while C_2–C_4 hydrocarbons, especially ethene, were formed as the major products at the expense of the C_5^+ hydrocarbons when the temperature was increased. Increasing the temperature from 350 to 550 °C led to a decrease in the selectivity for C_5^+ hydrocarbons from 53% to 6%, with a concomitant increase in the selectivity for ethene (from 1.9% to 26.6%) and propene (from 16.1% to 36.2%). Although the temperature had influence on the product distribution over SAPO-11 in a manner consistent with HZSM-22, there did not appear to be a significant variation in the product distribution over SAPO-11 with reaction temperature. Furthermore, increasing the temperature from 350 to 500 °C led to a slight decrease in the C_5^+ selectivity, as well as an increase in propene selectivity.

3.2.2. Deactivation of methanol conversion over HZSM-22 and SAPO-11

Figure 8 shows the GC-MS chromatograms and the amounts of deposited coke determined by TGA on HZSM-22 and SAPO-11 following their reactions at 350, 400, 450 and 500 °C. Naphthalene, phenanthrene, 9H-fluorene and tetraphene, as

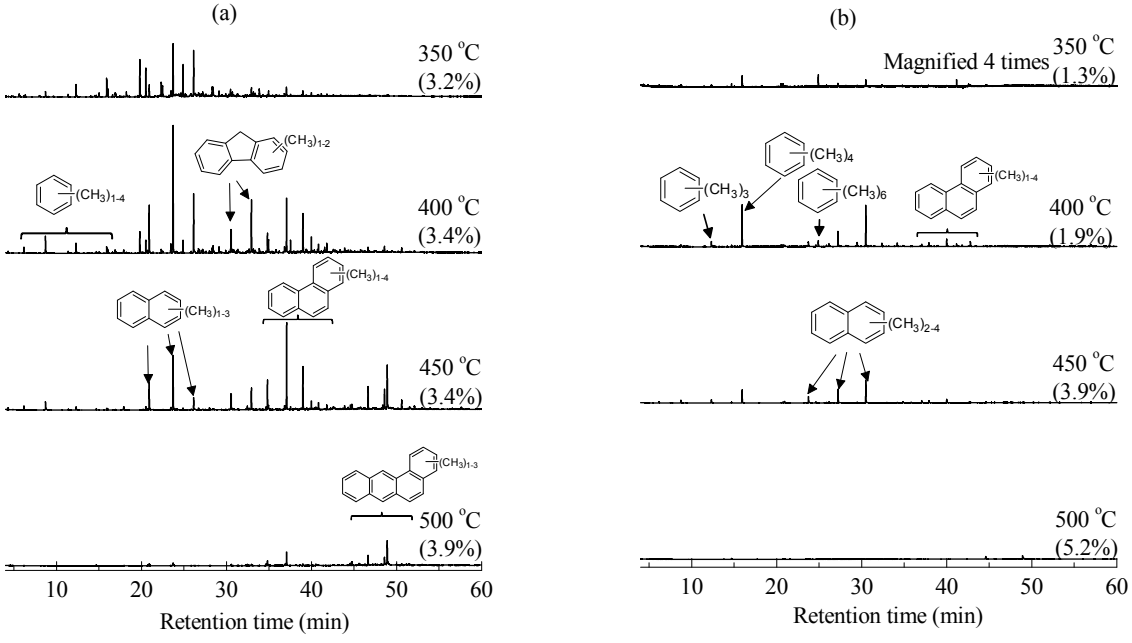

Fig. 8. GC-MS chromatograms of the organic species retained in HZSM-22 (a) and SAPO-11 (b) after the MTO reactions at various reaction temperatures with a methanol WHSV of 3.0 h^{-1} and a He/methanol ratio of 1.9. The coke amounts are shown in the brackets.

well as their methyl-substituted derivatives were identified as the main species to have been retained on deactivated HZSM-22. The main species retained on deactivated SAPO-11 were naphthalene, phenanthrene and their methyl-substituted derivatives. It can be seen from Fig. 8 that the concentration of the retained coke species detected by GC-MS varied with the reaction temperature. The concentrations of detected organic coke species increased to their maximum values at 400 and 450 °C over HZSM-22 and 400 °C over SAPO-11. The concentrations then decreased when the temperature was further enhanced up to 500 °C. However, the amounts of deposited coke determined by TGA increased steadily with increasing temperature, which indicates that graphitic coke species were being gradually formed and becoming dominant at high temperatures over both catalysts. It was subsequently concluded that these graphitic deposits, which were not soluble in dichloromethane and therefore not detected by GC-MS, were the leading cause of the deactivation of both catalysts at high temperatures. In contrast, the deactivation of both catalysts at low temperatures could be attributed to the blocking of the zeolite pores by condensed aromatic compounds based on the analysis of the concentrations of the retained coke species analyzed by GC-MS, as discussed above. The formation of more heavy hydrocarbons, including methyl-substituted phenanthrene and tetraphene, as the coke species over HZSM-22 compared with SAPO-11 could be the primary reason for the rapid deactivation of HZSM-22 relative to SAPO-11. It is noteworthy that the rapid deactivation behavior of methanol conversion over HZSM-22 relative to SAPO-11 at 400 °C could be related to the stronger acidic strength of HZSM-22 compared with SAPO-11.

These results therefore indicate that the rapid deactivation of HZSM-22 at relatively low temperatures, such as 400 °C, could be attributed to the blockage of the channel openings of the catalyst. With this in mind, we conducted *in situ* FTIR spectroscopy experiments to provide evidence to support this finding by monitoring changes in the Brönsted acidic sites during the conversion of methanol over HZSM-22. The spectra collected at 400 °C with time on stream are shown in Fig. 9. The two characteristic bands of the activated sample at 3740 and 3585 cm^{-1} were assigned to terminal silanol groups (Si(OH)) located on the external surface and framework bridging hydroxyl groups (Si(OH)Al), respectively, with the latter acting as the Brönsted acidic sites [46]. A new band appeared during the progress of the methanol reaction at 3136 cm^{-1}, which is assigned to the C-H stretching vibrations of the aromatic species and gradually increased in intensity with time on stream [47]. At the same time, there was a slight decrease in the intensity of the band derived from the bridging hydroxyl group at 3585 cm^{-1}, which indicates that the Brönsted acidic sites were being lost with the progress of the methanol reaction. After a reaction time of 15 min, the intensity of the peak at 3136 cm^{-1} reached a plateau, which implies that the reaction had ended because of the deactivation of the catalyst. However, the peak at 3585 cm^{-1} from the bridging hydroxyl groups could still be observed quite clearly. The consequences of these changes in the spectra for the aromatics formed during the reaction and the uncovered Brönsted acidic sites provide direct evidence to confirm the deactivation behavior of HZSM-22 during the MTH conversion. The blocking of the channels with polyaromatic compounds would lead to the rapid deactivation of the catalysts at low temperatures, which would prevent the methanol molecules from coming into contact with the remaining acidic sites inside the channel after the deactivation of the catalysts.

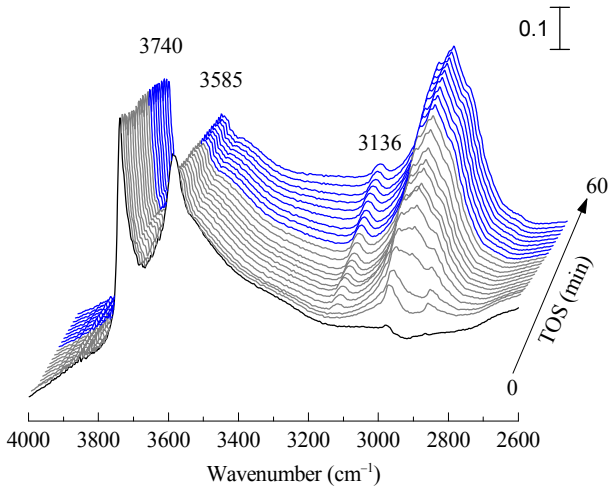

Fig. 9. *In situ* FTIR spectra for the conversion of methanol over HZSM-22 at 400 °C with a He/CH_3OH ratio of 18.

3.3. $^{12}C/^{13}C$-methanol switch experiments over HZSM-22 and SAPO-11

$^{12}C/^{13}C$-Methanol switch experiments were performed to elucidate the mechanism of the conversion of methanol over the two catalysts, HZSM-22 and SAPO-11, and the results of the isotopic distribution are shown in Fig. 10. Despite the differences in acid strength of the two catalysts, the isotopic switching experiments showed very similar isotopic distributions in the alkene products and the retained materials (methylated benzene) for both catalysts. The much higher ^{13}C content in the alkene products compared with the retained materials implied that ^{13}C atoms could be incorporated into alkenes with greater ease than heavy hydrocarbons, which suggests that the alkene cycle was dominant over the aromatic cycle in both catalysts. The slightly lower ^{13}C content in ethene compared with the C_{3+} alkenes could be related to the contribution of the arene cycle to the formation of ethene, although this pathway would make only a minor contribution to the formation of ethene [30]. Among the retained organics, the pentamethyl benzene (PentaMB) and hexamethyl benzene (HexaMB) materials found within SAPO-11 and HZSM-22, exhibited higher total ^{13}C contents than any of the other organic materials. However, these two polymethylated benzene molecules cannot act as efficient hydrocarbon pool species because of the limited chemical environment exerted by the 1-dimensional and 10-ring channel structures of the catalysts. Taken together, these results provide conclusive proof that the alkene methylation and cracking route is the dominating mechanism for the formation of alkenes over HZSM-22 and SAPO-11. These results are in good

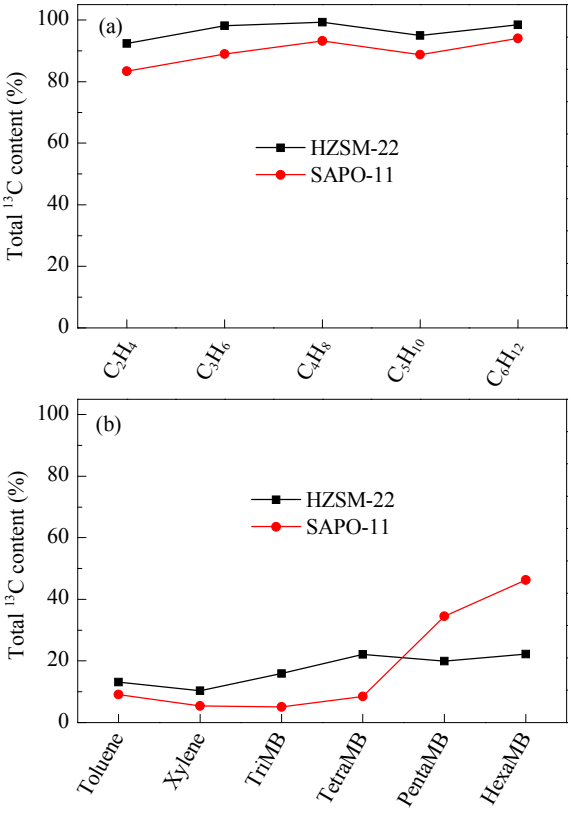

Fig. 10. Total ^{13}C contents in the effluent products (a) and retained materials (b) after a 15 min ^{12}C-methanol reaction followed by a 1 min ^{13}C-methanol reaction over HZSM-22 and SAPO-11 at 400 °C, with a WHSV of 2.0 g/(g·h) and a He/methanol ration of 10.1.

agreement with those of several previously published reports concerning the formation of alkenes over HZSM-22 [29–32].

3.4. Co-reaction of ^{13}C-methanol and ^{12}C-1-butene over HZSM-22 and SAPO-11

As discussed above, the results of the ^{12}C/^{13}C-methanol switching experiments demonstrated that the alkene-mediated mechanism can run as an independent process over HZSM-22 and SAPO-11. However, the effect of the Brönsted acidic strength of these catalysts on the conversion of methanol via the alkene methylation and cracking route remains unclear. We then proceeded to investigate the co-feeding of ^{13}C-methanol and ^{12}C-1-butene over HZSM-22 and SAPO-11 to determine the impact of the Brönsted acidic strengths of these catalysts on the methylation and cracking reaction and product distribution characteristics.

Methanol can be completely converted to hydrocarbons

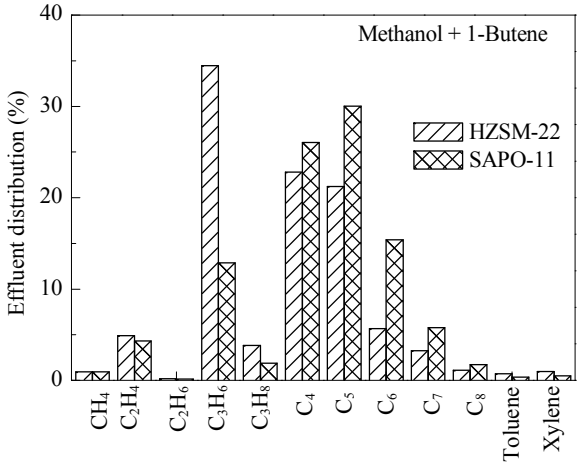

Fig. 11. Effluent product distributions for the conversion of methanol over HZSM-22 and SAPO-11 at 400 °C with a He/CH_3OH ratio of 7.

over HZSM-22 from neat methanol, as well as the co-reaction of methanol with 1-butene. However, the conversion of methanol over SAPO-11 was much lower than it was over HZSM-22, although the feeding of 1-butene into the reaction mixture as a co-reactant led to an increase in the conversion from 30.5% to 45.6%. The distribution of effluent products for the co-reaction of methanol with 1-butene over HZSM-22 and SAPO-11 is shown in Fig. 11. It is clear from these results that the majority of the effluent products formed over HZSM-22 were C_3–C_5 hydrocarbons. However, the product distribution shifted to heavier hydrocarbons (i.e., C_4–C_6 hydrocarbons) over SAPO-11. Furthermore, the selectivity for propene over HZSM-22 was much higher than it was over SAPO-11, whereas the selectivity for C_3^+ hydrocarbons over HZSM-22 was lower than it was over SAPO-11. These differences indicated that the cracking reaction for the formation of light alkenes, especially propene, was favored over HZSM-22 compared with SAPO-11, despite the fact that the methylation of 1-butene occurs for the generation of higher alkenes.

The distribution of the ^{12}C content in the effluent products was determined by GC-MS, and the results are shown in Table 3. For the reaction over HZSM-22, the ^{12}C atoms originating from ^{12}C-1-butene were mainly located in the C_3–C_5 hydrocarbon products, which accounts for 31.85%, 22.78% and 24.47% of the carbon atoms based on ^{12}C-1-butene. For SAPO-11, the C_4–C_6 hydrocarbons contained the majority of the ^{12}C atoms and accounted for 38.68%, 37.59% and 15.27% of the ^{12}C atoms, respectively. These findings therefore provided further evidence that the conversion of methanol occurred via the alkene-mediated pathway and indicated that the acidic strength had a significant impact on the cracking reactivity of heavy

Table 3
^{12}C distribution of co-feeding experiments of ^{13}C-methanol and ^{12}C-Butene (5.3 based on C atom) over HZSM-22 and SAPO-11.

Catalyst	^{12}C distribution in reactor outlet products (%)											
	C_1^0	$C_2^=$	C_2^0	$C_3^=$	C_3^0	C_4	C_5	C_6	C_7	C_8	Toluene	Xylene
HZSM-22	0	4.26	0	31.85	2.38	22.78	24.47	9.70	2.70	0.83	0.48	0.56
SAPO-11	0	0	0	3.10	0.18	38.68	37.59	15.27	4.08	0.95	0.06	0.08

hydrocarbons, leading to the differing product distributions. Based on these results, we can conclude that the acidic properties of zeolite catalysts have been identified as a key factor for their reactivity and product distribution in the MTH reaction, and that the flexible adjustment of these acidic properties could facilitate the optimization of catalytic performance.

4. Conclusions

The influence of catalyst acidity on the methanol reaction and deactivation mechanisms of zeolite catalysts has been systematically investigated using two one-dimensional 10-ring catalysts, HZSM-22 and SAPO-11. Comparative studies over these two catalysts with different acidities indicated that the differences in the acidic strengths of these catalysts had a significant impact on their activity and stability, as well as their product distribution and deactivation patterns. The more acidic HZSM-22 catalyst exhibited higher reactivity than SAPO-11. However, the moderate acidic strength of SAPO benefited the stability of the MTH reaction. The blockage of the pores of these catalysts by polyaromatic compounds was discovered to be responsible for the deactivation of the two catalysts at relatively low temperatures. In contrast, the deactivation of these catalysts at high temperatures was attributed to graphitic coke deposition on the outer surface of the catalysts. The results of a $^{12}C/^{13}C$-methanol switch experiment showed that the conversion of methanol over the two catalysts followed an alkene methylation and cracking route. The results of co-feeding experiments involving ^{13}C-methanol and ^{12}C-butene suggested that the cracking of higher hydrocarbons was promoted over HZSM-22 because of its higher acidic strength compared with SAPO-11. This resulted in C_3–C_5 hydrocarbons as the major products for HZSM-22, while C_{5+} hydrocarbons were formed as the major products for SAPO-11.

References

[1] Olsbye U, Svelle S, Bjorgen M, Beato P, Janssens T V W, Joensen F, Bordiga S, Lillerud K P. *Angew Chem Int Ed,* 2012, 51: 5810
[2] Wei Y X, Zhang D Z, Liu Z M, Su B L. *Chin J Catal,* 2012, 33: 11
[3] Stöcker M. *Microporous Mesoporous Mater*, 1999, 29: 3
[4] Tian P, Wei Y X, Ye M, Liu Z M. *ACS Catal,* 2015, 5: 1922
[5] Hemelsoet K, Van der Mynsbrugge J, De Wispelaere K, Waroquier M, Van Speybroeck V. *ChemPhysChem,* 2013, 14: 1526
[6] Liang J, Li H Y, Zhao S, Guo W G, Wang R H, Ying M L. *Appl Catal,* 1990, 64: 31
[7] Koempel H, Liebner W. *Stud Surf Sci Catal,* 2007, 167: 261
[8] Chang C D. *Catal Today,* 1992, 13: 103
[9] Yurchak S. *Stud Surf Sci Catal,* 1988, 36: 251
[10] Topp-Jørgensen J. *Stud Surf Sci Catal,* 1988, 36: 293
[11] Chen J Q, Bozzano A, Glover B, Fuglerud T, Kvisle S. *Catal Today,* 2005, 106: 103
[12] Dahl I M, Kolboe S. *J Catal,* 1996, 161: 304
[13] Dahl I M, Kolboe S. *J Catal,* 1994, 149: 458
[14] Dahl I, Kolboe S. *Catal Lett,* 1993, 20: 329
[15] Arstad B, Kolboe S. *J Am Chem Soc,* 2001, 123: 8137
[16] Song W G, Haw J F, Nicholas J B, Heneghan C S. *J Am Chem Soc,* 2000, 122: 10726
[17] Wang C M, Wang Y D, Liu H X, Xie Z K, Liu Z P. *J Catal,* 2010, 271: 386

Graphical Abstract

Chin. J. Catal., 2015, 36: 1392–1402 doi: 10.1016/S1872-2067(15)60953-6

Methanol to hydrocarbons reaction over HZSM-22 and SAPO-11: Effect of catalyst acid strength on reaction and deactivation mechanism

Jinbang Wang, Jinzhe Li, Shutao Xu, Yuchun Zhi, Yingxu Wei *, Yanli He, Jingrun Chen, Mozhi Zhang, Quanyi Wang, Wenna Zhang, Xinqiang Wu, Xinwen Guo *, Zhongmin Liu *
Dalian University of Technology; Dalian Institute of Chemical Physics, Chinese Academy of Sciences; University of Chinese Academy of Sciences

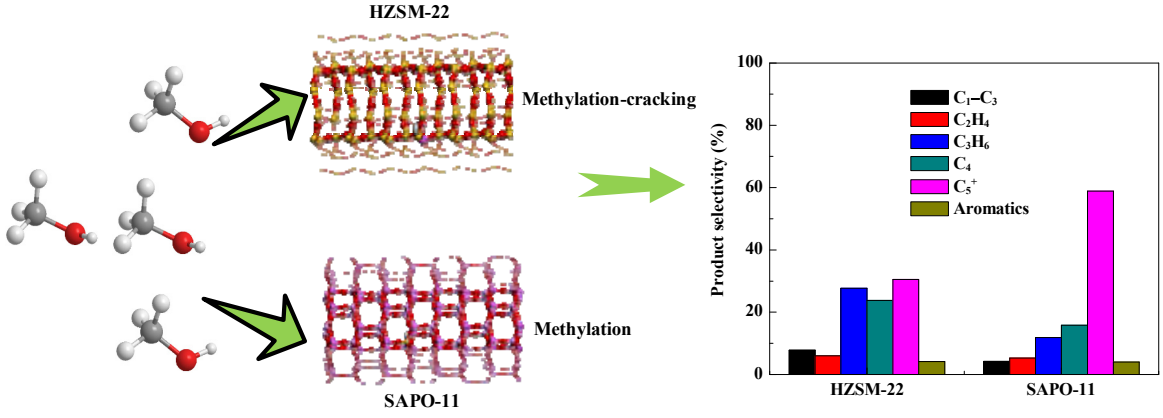

Comparative studies over HZSM-22 and SAPO-11 have demonstrated the importance of the acidity of a catalyst on its activity and stability, as well as its product distribution and deactivation patterns for the conversion of methanol following the alkene methylation and cracking route.

[18] Hereijgers B P C, Bleken F, Nilsen M H, Svelle S, Lillerud K P, Bjørgen M, Weckhuysen B M, Olsbye U. *J Catal,* 2009, 264: 77
[19] Xu S T, Zheng A M, Wei Y X, Chen J R, Li J Z, Chu Y Y, Zhang M Z, Wang Q Y, Zhou Y, Wang J B, Deng F, Liu Z M. *Angew Chem Int Ed,* 2013, 52: 11564
[20] Wulfers M J, Jentoft F C. *ACS Catal,* 2014, 4: 3521
[21] Li J Z, Wei Y X, Chen J R, Xu S T, Tian P, Yang X F, Li B, Wang J B, Liu Z M. *ACS Catal,* 2015, 5: 661
[22] Wang C M, Wang Y D, Xie Z K, Liu Z P. *J Phys Chem C,* 2009, 113: 4584
[23] Bjørgen M, Olsbye U, Petersen D, Kolboe S. *J Catal,* 2004, 221: 1
[24] Li J Z, Wei Y X, Chen J R, Tian P, Su X, Xu S T, Qi Y, Wang Q Y, Zhou Y, He Y L, Liu Z M. *J Am Chem Soc,* 2012, 134: 836
[25] Li J Z, Wei Y X, Xu S T, Tian P, Chen J R, Liu Z M. *Catal Today,* 2014, 226: 47
[26] Svelle S, Joensen F, Nerlov J, Olsbye U, Lillerud K P, Kolboe S, Bjørgen M. *J Am Chem Soc,* 2006, 128: 14770
[27] Bjorgen M, Svelle S, Joensen F, Nerlov J, Kolboe S, Bonino F, Palumbo L, Bordiga S, Olsbye U. *J Catal,* 2007, 249: 195
[28] Svelle S, Olsbye U, Joensen F, Bjørgen M. *J Phys Chem C,* 2007, 111: 17981
[29] Teketel S, Svelle S, Lillerud K-P, Olsbye U. *ChemCatChem,* 2009, 1: 78
[30] Teketel S, Olsbye U, Lillerud K-P, Beato P, Svelle S. *Microporous Mesoporous Mater,* 2010, 136: 33
[31] Li J Z, Wei Y X, Liu G Y, Qi Y, Tian P, Li B, He Y L, Liu Z M. *Catal Today,* 2011, 171: 221
[32] Li J Z, Wei Y X, Qi Y, Tian P, Li B, He Y L, Chang F X, Sun X D, Liu Z M. *Catal Today,* 2011, 164: 288
[33] Yuen L-T, Zones S I, Harris T V, Gallegos E J, Auroux A. *Microporous Mater,* 1994, 2: 105
[34] Bleken F, Bjørgen M, Palumbo L, Bordiga S, Svelle S, Lillerud K-P, Olsbye U. *Top Catal,* 2009, 52: 218
[35] Westgård Erichsen M, Svelle S, Olsbye U. *J Catal,* 2013, 298: 94
[36] Yang G J, Wei Y X, Xu S T, Chen J R, Li J Z, Liu Z M, Yu J H, Xu R R. *J Phys Chem C,* 2013, 117: 8214
[37] Guisnet M, Costa L, Ribeiro F R. *J Mol Catal A,* 2009, 305: 69
[38] Buchholz A, Wang W, Xu M, Arnold A, Hunger M. *Microporous Mesoporous Mater,* 2002, 56: 267
[39] Li B, Tian P, Qi Y, Zhang L, Xu S T, Su X, Fan D, Liu Z M. *Chin J Catal,* 2013, 34: 593
[40] Jiang Y J, Huang J, Dai W L, Hunger M. *Solid State Nucl Magn Reson,* 2011, 39: 116
[41] Müller M, Harvey G, Prins R. *Microporous Mesoporous Mater,* 2000, 34: 281
[42] Zheng A M, Huang X J, Wang Q, Zhang H L, Deng F, Liu S B. *Chin J Catal,* 2013, 34: 436
[43] Hunger M, Anderson M W, Ojo A, Pfeifer H. *Microporous Mater,* 1993, 1: 17
[44] Hunger M. *Catal Rev,* 1997, 39: 345
[45] Zhang W P, Ma D, Liu X C, Liu X M, Bao X H. *Chem Commun,* 1999: 1091
[46] Borade R B, Adnot A, Kaliaguine S. *Zeolites,* 1991, 11: 710
[47] Sousa Z S B, Cesar D V, Henriques C A, Teixeira da Silva V. *Catal Today,* 2014, 234: 182

Page numbers refer to the contents in the print version, which include both the English version and extended Chinese abstract of the paper. The online version only has the English version. The pages with the extended Chinese abstract are only available in the print version.